Cryst. Res. Technol. **42**, No. 3, 266 – 274 (2007) / **DOI** 10.1002/crat.200610811

Photoacoustic studies on optical and thermal properties of p-type and n-type nanostructured porous silicon for (100) and (111) orientations

R. Srinivasan[1], M. Jayachandran[2], and K. Ramachandran*[3]

[1] Department of Physics, Thiagarajar College, Madurai - 625 009, India
[2] ECMS Division, Central Electrochemical Research Institute, Karaikudi – 630 006, India
[3] School of Physics, Madurai Kamaraj University, Madurai – 625 021, India

Received 7 August 2006, revised 29 September 2006, accepted 7 October 2006
Published online 10 February 2007

Key words porous silicon, thermal conductivity, photoacoustic spectroscopy, phonon confinement.
PACS 81.70.Cv, 78.55.Mb

Nanostructured p-type and n-type porous silicon samples were prepared for (100) and (111) orientations and a systematic study is carried out on the effects of orientations, dopant type (boron and phosphorous), current density (20 and 30mA/cm^2) and etching time on the formation, optical and thermal properties by photoacoustic spectroscopy.

1 Introduction

Room temperature luminescence in the visible region by porous silicon (PS), after Canham's discovery had triggered research all over the world on porous materials [1-2]. The use of PS as an efficient material in optoelectronics, optical interconnections and electroluminescent devices leads to ultra-large-scale-integrated (ULSI) applications. Also this PS is being used in micromachining [3], in which it acts as sacrificial layer and biomaterial [4] in different applications.

Blonskij et al. [5] and Ferreira da Silva et al. [6] investigated the optical and thermal properties of p-type porous silicon by photoacoustics. Prabakaran et al. [7] studied the optical and micro structural investigations of n-type porous silicon (100).

Qing Shen et al. [8] reported the dependence of thermal conductivity of PS on porosity by photoacoustic technique and showed that the thermal conductivity of PS films decreases as the porosity increases. Jayachandran et al. [9] synthesized porous silicon nanostructures for photoluminescence devices and observed that at room temperature, photoluminescence depends on anodization current density and time. Since PS is also a very good thermal insulator, studies on thermal properties have started coming. Lettieri et al. [10] made optical investigations on thermal conductivity in n- and p-type porous silicon by means of photoacoustic and optical pump-probe techniques and reported that n-PS has a complex morphology, in which mesophases, nanophases and macrophases coexist. In p-type, thermal conductivity is lower than n-type PS.

Ebothe et al. investigated [11] acoustically induced optical second harmonic generation in hydrogenated amorphous silicon films (AISHG) and demonstrated substantial acoustical induced non-linear optical effects in amorphous silicon films; i.e., with increasing acoustical power, the optical SHG of Gd : YAB laser light (λ = 2.03 μm) increases and reaches its maximum value at an acoustical power density of about 2.10 W cm^{-2}.

* Corresponding author: e-mail: thirumalchandran@yahoo.com, r_srini2067@yahoo.co.in

Electrical properties of macroporous silicon structures were studied by Karachevtseva et al. [12] and reported that the electron conductivity and concentration decrease with increase in pore diameter and increase in pore concentration.

Zhao Yue et al. [13] studied the surface morphology and I-V curves of porous silicon devices and showed that during etching process, the etching rate of the Si (111) crystal plane is about two orders of magnitude larger than that of the (100) and (110) crystal planes.

An investigation of electrical properties of porous silicon for different current densities was made by Algun et al. [14] and had concluded that both pore radius and concentration would grow when current density is increased.

Eventhough porous silicon had been extensively studied in the recent past, a complete study on the optical and thermal properties in both n-type porous silicon (n-PS) and p-type porous silicon (p-PS) for different orientations (100) and (111) is not well documented in the literature and also the few reported results had no uniqueness in their values [6] on thermal properties. So the present work is focused to study the dependence of optical and thermal properties of porous silicon on orientations, dopant type, current density and anodization time.

2 Preparation of porous silicon

Samples used in this study are boron and phosphorous doped crystalline silicon (c-Si) wafers (thickness 525 μm and resistivity 1-3 Ω cm) grown by Czochralski (CZ) method in (100) and (111) orientations. Initially these crystals are characterized by XRD and FTIR. The cell parameters found by XRD are 5.4255, 5.4309 and 5.4321A, which are compared with the parameters of silicon (JCPDS file). FTIR spectra showed an absorption peak at 1107 cm^{-1} which is identified from literature [15] as stretched vibration of Si-O-Si; that is due to interstitial oxygen in (111).

The porous samples were then prepared by electrochemical anodic dissolution of doped silicon in 48% hydrofluoric acid, H_2O and ethanol with platinum electrode as cathode. The electrolyte was prepared by mixing HF (48%), H_2O and ethanol in 1:1:2 ratios. The porous layers on the surface of these samples were prepared at current densities of 30mA/cm^2 with etching time 30min and 20mA/cm^2 with etching times of 10, 30 and 60min and for convenience of discussions, these samples are identified as follows. For example an n-Si with (100) orientation was etched with a current density of 30mA/cm^2 (from a constant current source) and etching time 30 minutes is identified as n-PS0; similarly for p-PS0 and other samples as given table 1.

Table 1 Classification of the samples.

S.No	Type	Orientation	Current density (mA/cm^2)	Etching time (min)	Sample Name
1	n	(100)	30	30	n-PS0
2			20	10	n-PS01
3				30	n-PS02
4				60	n-PS03
5	n	(111)	30	30	n-PS1
6			20	10	n-PS11
7				30	n-PS12
8				60	n-PS13
9	p	(100)	30	30	p-PS0
10			20	10	p-PS01
11				30	p-PS02
12				60	p-PS03
13	p	(111)	30	30	p-PS1
14			20	10	p-PS11
15				30	p-PS12
16				60	p-PS13

The atomic force micrographs (AFM) were taken for c-Si and porous silicon by Siemens Atomic Force Microscope to confirm the porosity. Only some typical AFM pictures (n-PS0 and p-PS0) are given here. The average radius and interparticle distance of p-PS0 are found to be 6.12 nm and 30nm. The different levels of porosity could be clearly seen in the pictures (Figs. 2 and 4).

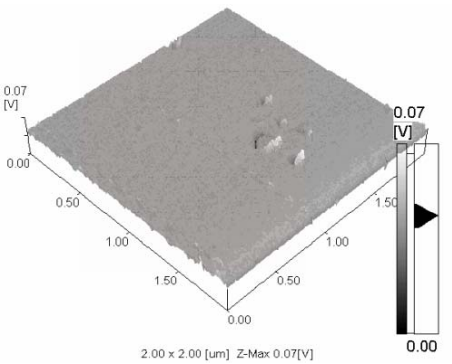

Fig. 1 AFM image of n-type Silicon (100).

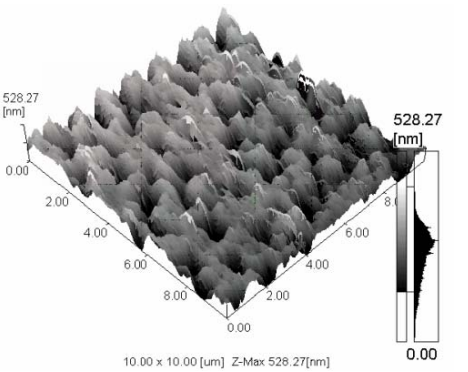

Fig. 2 AFM image of n-PS0.

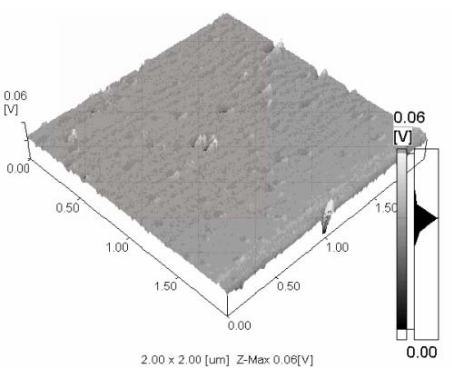

Fig. 3 AFM image of p- type Silicon (100).

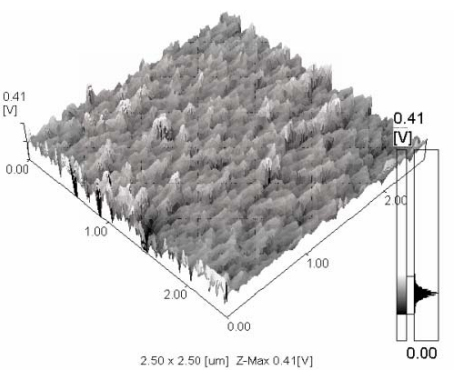

Fig. 4 AFM image of p-PS0.

3 Photoluminescence

Photoluminescence emission spectra for all the above porous silicon samples, are recorded using a spectroflurophotometer (Shimadzu RF-5000) and shown in figure 5.

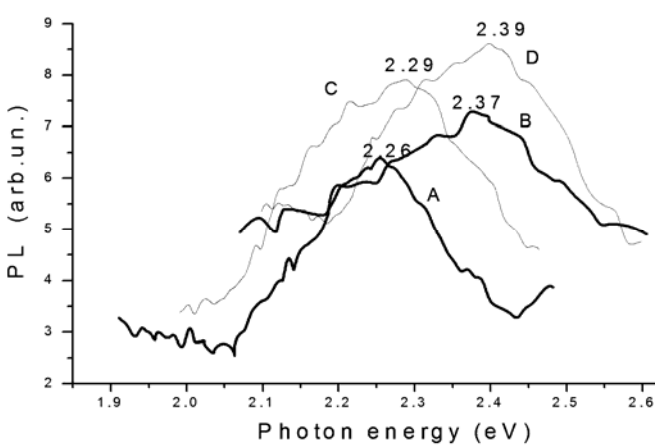

Fig. 5 Photoluminescence spectra for the various PS samples. **A**: n-PS0, **B**: n-PS1, **C**: p-PS0 and **D**: p-PS1.

From figure 5 the band gap is calculated for each sample from the PL emission. Firstly it is observed, that there is a blue shift in band gap of p-PS1 (D) when p-PS0 (C) is compared. Similarly n-PS1 (B) is blue shifted than n-PS0 (A) (when compared to c-Si, the blue shift in p-PS and n-PS are atleast 2-fold). The above results imply that the shift in (111) orientation of PS is more compared to (100). This shift can be explained from the reduction in particle size or the porosity effect.

The particle size can be calculated from the band gap (the details of these calculations are discussed later in the photoacoustic section) observed from PL spectra and the band gaps are given in table 2. The porosity is calculated by measuring weight changes Δm of each silicon wafer before and after the electrochemical etching. It is reported that [7] blue shift in band gap (band gap widening) is due to reduction in the size of the Si nanocrystallite with increasing etching time, but it is also reported that [8] porosity increases largely with increase in etching time. It is seen from table 2, that the particle size of (111) grown in PS samples are low compared to their respective PS samples in (100) orientation, under identical etching parameters. This is also reason for the shift in band gap observed in (111) orientation than (100). Hence the blue shift shown in (111) orientation is expected to be because of decrease in particle size and increase in porosity as could be seen from table 2.

Similarly, the observed shift in p-PS over n-PS (D over B and C over A) can also be understood in terms of the particle size and porosity as seen from table 2. But it is also noticed that shift observed in (111) oriented p-PS is more than the shift observed in n-PS.

Table 2 Band gap and particle size of PS samples from PL spectra. (Error in measurements is less than 1%).

Sample Name	In Fig. 5	Band gap (eV)	Particle size (nm)	Porosity (%)
n-PS0	A	2.26	6.28	60
n-PS1	B	2.37	5.90	67
p-PS0	C	2.29	6.17	64
p-PS1	D	2.39	5.84	70

For the other samples also, such measurements on band gaps were done and tabulated in Table 3. It is seen that as the etching time increases the band gap increases and so a reduction in particle size for both orientations of n-PS. Further it is noticed from the table that porosity increases with increase in etching time, which is in agreement with the results of Qing Shen et al. [8]. At the same time the porosity of (111) oriented PS samples are more than the (100) as already reported by Zhao et al. [13] that during the etching process, the etching rate of the Si (111) crystal plane is about two orders of magnitude larger than that of the (100) and (110) planes. Further, as the etching of silicon in our study is confined to low current densities and, the electrolyte used is a mixture of HF, H_2O and ethanol with 1:1:2 ratio (not with HF alone), no appreciable change in thickness was observed. But the change in porosity was observed with current densities and etching periods.

Table 3 Band gap and particle size of n-PS for (111) and (100) orientations at a constant current density of 20mA/cm^2 for various etching periods by photoluminescence. (Error in measurements is less than 1%).

n-PS (100) orientation				n-PS (111) orientation			
Sample	Band gap (eV)	Particle size (nm)	Porosity %	Sample	Band gap (eV)	Particle size (nm)	Porosity %
n-PS01	2.17	6.63	43	n-PS11	2.20	6.51	47
n-PS02	2.19	6.55	49	n-PS12	2.23	6.39	53
n-PS03	2.24	6.35	57	n-PS13	2.32	6.07	61

To confirm these results further, ampere-volt (I-V) characteristics are carried out on a set of samples (n-PS0 and p-PS0) and the results are shown in figure 6. It is seen from figure 6, that the lesser current flows in p-PS0 than n-PS0 implying that the electrical conductivity of n-PS0 is higher than p-PS0. i.e., the electrical resistivity of p-PS0 is higher than n-PS0. This can be directly correlated with the work of Lettieri et al. [10], where higher

thermal conductivity in n-PS is reported. Further it is reported in literature [14] that pore concentration increases with current density and higher resistivity is a result of carriers trapped at the pore walls. It is seen that the pore concentration of p-PS0 is higher than the n-PS0 as observed from AFM figures. Also the lower thermal conductivity of p-PS is expected because of its higher porosity (64%) than that of n-PS (60%) as the thermal conductivity of PS decreases with increase in porosity [8].

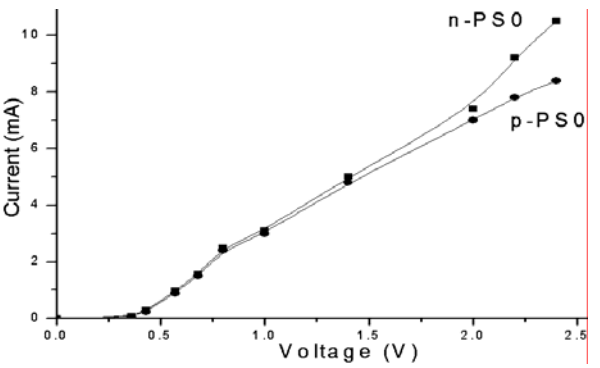

Fig. 6 I–V characteristics of n-PS0 and p-PS0 (current density 30mA/cm^2, 30min).

4 Photoacoustic spectroscopy(PAS)

PAS has become an important tool in the characterization of semiconductors. It is a nondestructive and contactless technique and is unique in being a direct monitor of nonradiatiave de-excitation processes. One of the important features of PAS is its potential for detecting subsurface variations of both optical and thermal properties of a sample, including the elastic properties. These advantages have led to the current widespread use of the technique [16-19]. In the case of semiconductors, the photoacoustic signal provides information regarding the carrier transport properties as well as thermal properties.

Many reports are available in literature for PS by photoacoustics, as given in the introduction, but no detailed comparisons on type and orientation of PS are reported. Here this is carried out and compared not only with the reported PA results, but also with our PL and V-I studies.

PAS experimental set-up The present PA spectrometer has a 450 W xenon lamp FL-1039 (Jobin Yvon, USA) as source, a monochromator (TRIAX series, Jobin Yvon, USA) for different wavelengths, a chopper (PAR chopper) in the frequency range 10 Hz–2 kHz and a PA cell. A condenser microphone was used as the detector and a lock-in amplifier (7225 PAR, USA) to display the PA signal.

When a modulated light is absorbed by the sample located in a sealed cell, the nonradiative decay of the absorbed light produces a modulated transfer of heat to the surface of the sample. This modulated thermal gradient produces pressure waves in the gas inside the cell that can be detected by the microphone attached to the cell. The resulting signal depends not only on the amount of heat generated in the sample (and hence, on the optical absorption coefficient and the light-into-heat conversion efficiency of the sample) but also on how the heat diffuses through the sample [18].

Thermal diffusivity and conductivity Thermal diffusivity (α) is the rate of periodic heating or transient heat propagation through a medium. To determine the thermal diffusivity of the above PS samples, the PA signal amplitude is recorded as a function of chopping frequency.

The thermal diffusivity (α) is determined from the thermal diffusion model for the photoacoustic effect, where for an optically opaque sample, the pressure fluctuations are given by [19],

$$\delta p = \gamma p_0 I_0 \left(\alpha_g \alpha_s\right)^{1/2} \exp j\left(\omega t - \frac{\pi}{2}\right) / 2\pi T_0 l_g \kappa_s f \sinh\left(l_s \sigma_s\right) \tag{1}$$

where γ is the specific heat ratio of air, P_0 the ambient pressure, I_0 the incident light beam intensity, T_0 the room temperature, f the chopping frequency and l_i, k_i and α_i are the thickness, thermal conductivity and thermal diffusivity of material i respectively.

The subscript *i* denotes either sample (s) or gas (g) regions and $\sigma_i = (1+j)\,a_i$ with $a_i = \left(\frac{\pi f}{\alpha_i}\right)^{1/2}$ is the complex thermal diffusion coefficient of material '*i*'. Particularly, for an optically opaque and thermally thick sample ($l_s\sigma_s >> 1$), the expression for the photoacoustic amplitude is given by,

$$S = \frac{A}{f}\exp(-af^{1/2}) \tag{2}$$

where the constant *A*, apart from geometric constants, include factors such as the light intensity, room temperature, gas thermal properties and $a = \left(\frac{\pi l_s^2}{\alpha_s}\right)^{1/2}$. From the slope of the graph connecting *l*n(*f*. S) and $\sqrt{f}$, thermal diffusivity of the sample is deduced. Thermal conductivity is then calculated using the relation

$$\kappa = \alpha\rho C_p \text{ in units of W/m-K} \tag{3}$$

where ρ is the density and C_p is the specific heat capacity of c-Si.

In the experiment the PA amplitude is measured by varying the chopping frequency and graphs are drawn between $\sqrt{f}$ and ln(S * *f*), where *f* is the chopping frequency and S is the photoacoustic amplitude. To start with, this is carried out for p- and n-type c-Si for (100) and (111) orientations and then for porous samples. The graphs plotted for n-PS12 and p-PS12 are shown in figures 7 and 8 respectively. The thermal diffusivity (α) and then conductivity (k) were calculated using the slope from the graph. Similar measurements were done on other samples. The measurements are with an accuracy of less than ±1% at room temperature.

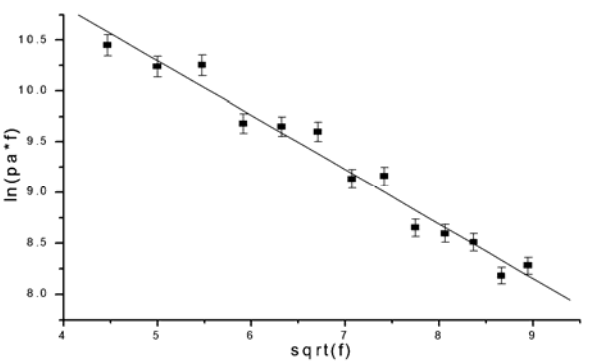

Fig. 7 Depth profile for n- PS12 (f-chopper frequency and S-amplitude of PA signal).

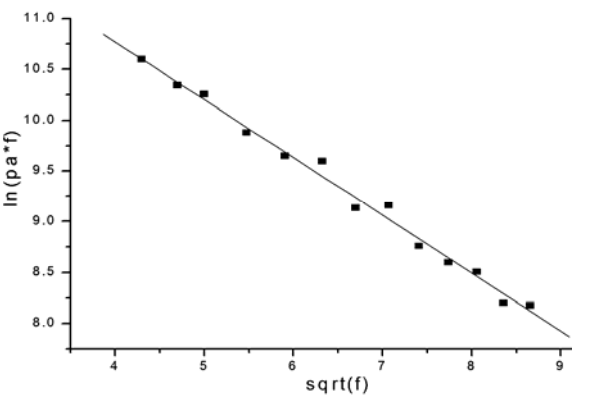

Fig. 8 Depth profile for p- PS12 (f-chopper frequency and S-amplitude of PA signal).

Table 4 Thermal properties of n-type and p-type silicon and undoped silicon(c-Si).

Doped silicon	Thermal properties	
	Thermal diffusivity x10^{-4} (m^2/s)	Thermal conductivity (W/m-K)
n-Si(111)	0.28	45.0
n-Si(100)	0.25	40.0
p-Si(111)	0.26	43.0
p-Si(100)	0.23	37.0
c-Si (Ref.20)	0.80	130.0

Table 4 shows the values of thermal diffusivity and conductivity for n- and p – type c-Si for (100) and (111) orientations and undoped bulk silicon. It is observed that the thermal diffusivities and conductivities of these samples are much lower than the undoped crystalline silicon. This can be explained as follows. The defects due to (i) interstitial oxygen [15] in (111) orientation grown crystal and (ii) dopants in c-Si [21] are responsible for

the decrease in thermal properties i.e., multiple scattering of donors with static imperfections lead to decrease in mean free path and hence thermal conductivities, as the thermal properties depend very much on the lattice properties.

Table 5 gives the thermal conductivity of PS samples. It is seen that, p-PS samples have lower thermal conductivity than n-PS. The lower value is as a result of decrease in mean free path due to the phonon confinement in crystallite; i.e., when the phonon mean free path is less than the crystallite size, phonons are confined and so the thermal conductivity is reduced. Jie Zou et al. [22] investigated phonon heat conduction in a semiconductor nanowire and reported that phonon confinement and boundary scattering lead to a significant decrease of the lattice thermal conductivity. These results are in agreement with the results of Litttieri et al [10]. Also the lower thermal conductivities in (111) oriented PS over (100) are due to the interstitial oxygen as mentioned earlier.

It is also noticed from table 5 that there is drastic one order decrease in thermal conductivities of PS samples compared to crystalline doped silicon. Phonon confinement is the prime reason for the drastic decrease of thermal conductivity of PS than c-Si. Further, the role of phonon sub-systems in the observed effects was also analysed and no electron-phonon anharmonicity is observed in these cases. This due to the fact, that the electron-phonon interaction will be observed only at high temperatures, not at room temperature. This has been confirmed by thermal expansion studies on porous samples and bulk samples.

Table 5 The thermal conductivity of n-PS and p-PS in (111) and (100) orientations, prepared at a current density 20mA/cm^2, for different etching times. (Error in measurement is less than 1%).

n-PS (100) and (111) orientations				p-PS (100) and (111) orientations			
	Thermal conductivity (W/m-K)				Thermal conductivity (W/m-K)		
Sample	Present work	Looyenga theory	Porosity %	Sample	Present work	Looyenga theory	Porosity %
n-PS01	8.31	8.33	43	p-PS01	7.33	7.15	45
n-PS02	5.38	5.96	49	p-PS02	4.89	5.06	51
n-PS03	3.59	3.57	57	p-PS03	3.10	2.75	60
n-PS11	6.20	5.96	47	p-PS11	5.22	4.91	49
n-PS12	4.73	4.15	53	p-PS12	4.10	3.60	54
n-PS13	2.93	2.37	61	p-PS13	1.96	1.73	64

To confirm the measured values of thermal conductivities of PS, these values are computed from Looyenga effective medium model [10, 23] with porosity p, but using $K_{eff} = fg_0K_s$, where f=1-p, g_0 is the fraction of interconnected solid phase, $g_0 = f^2$ and K_s is the thermal conductivity of solid phase. The calculated values are in good agreement with the experimental results for thermal conductivity. Thus the promising application of PS as silicon based thermal insulator in thermal effect micro-devices and micro-systems based on its low thermal conductivity has been identified and the above results suggest that for better thermal insulation, p-PS of (111) orientation is quite useful.

5 Photoacoustic spectrum

The PA spectra were recorded by observing the PA signal as a function of the wavelength of the incident beam for constant modulation frequency for p-PS and n-PS samples. The spectra were normalized using the PA spectrum of carbon black. The PA spectra of n-PS0, n-PS1, p-PS0 and p-PS1 are shown in figure 9. The band gap energies and particle sizes of these samples are calculated and given in table 6.

The size of the particle has been worked out from the well known equation (4) [24],

$$E_{gn} = \left[E_{gb}^2 + \left\{ \frac{2h^2 E_{gb} \left(\frac{\pi}{R} \right)^2}{m^*} \right\} \right]^{1/2} \tag{4}$$

where, E_{gb} is band gap of bulk semiconductor (1.11 for Si), R is the particle radius, m* is the effective mass of the electron and E_{gn} is the band gap for the nano system.

This equation is a well known and successful expression to explain the size of the particles down to about 3 nm and is derived explicitly by Wang et al. (24) following a molecular orbital theory and effective mass approximation. They have first studied the size of the particle by X ray diffraction for PbS particles. Scherrer's equation was used to find the size, involving the half width of the diffraction spectrum. The agreement with eqn. (4) was so good that the researchers started using this eqn. (4) for the size of the particle after Wang et al. [24].

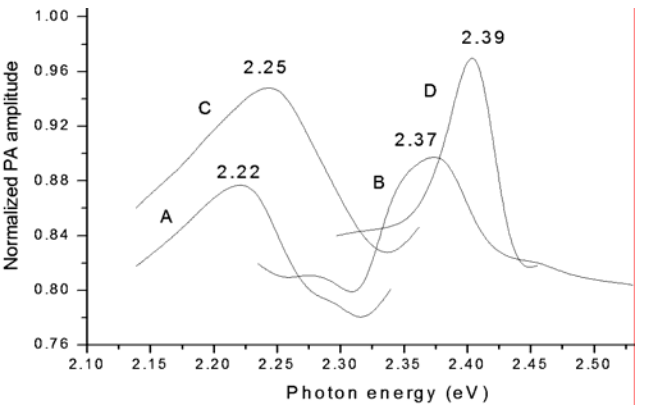

Fig. 9 PA spectra for various PS samples, A: n-PS0, B: n-PS1, C: p-PS0, D: p-PS1.

The PA spectra recorded for the n- and p-PS samples are shown in figure 9. A shift in band gap of (111) oriented PS samples is high over (100) orientation as observed in PL spectra. This shift is more in p-PS over n-PS for both orientations. The band gap and particle size of these samples are computed from PA spectra and given in table 6. These are similar to the results shown by PL spectra and the band gap energies found in the present work are consistent with PA energies shown by Ferreria et al. [6].

Table 6 Band gap and particle size of various PS samples by PA spectra. (Error in measurement is less than 1%).

n- and p-PS in (100) and (111) orientations			
Sample	Band gap (eV)	Particle size (nm)	Porosity %
n-PS0	2.22	6.43	60
n-PS1	2.37	5.90	67
p-PS0	2.25	6.32	64
p-PS1	2.39	5.84	70

The band gaps of n-PS computed from PA spectra for various etching periods are given in table 7 along with the particle size. These values show that band gaps in (111) orientation are higher compared to (100) which is consistent with the results of PL. The shift in optical band gaps of the PS layers from that of crystal Si (1.11eV) indicates a stronger quantum confinement of carriers in the PS layers due to the smaller mentions of the PS microcrystallite. The shift in band gap among these samples implies a reduction in the size of the silicon crysatllite with increasing etching time and thus leads to increase in porosity. These results are also in agreement with PL results.

Table 7 Band gap and particle size of n-PS for different orientations and etching periods. (Error in measurement is less than 1%).

n-PS (100) orientation				n-PS (111) orientation			
Sample	Band gap (eV)	Particle size (nm)	Porosity %	Sample	Band gap (eV)	Particle size (nm)	Porosity %
n-PS01	2.19	6.55	43	n-PS11	2.25	6.32	47
n-PS02	2.21	6.47	49	n-PS12	2.27	6.24	53
n-PS03	2.26	6.28	57	n-PS13	2.31	6.10	61

6 Conclusion

n- and p-type c-Si are grown in (100) and (111) orientations by CZ technique and porous layers are prepared for different current densities and etching periods. The samples are then characterized by PL and I-V curves. Though many reports are available in literature for PS by photoacoustics, but no detailed comparisons on type and orientation of PS are reported. Here this is carried out and compared not only with the reported PA results, but also with our PL and I-V studies. The PL and PA results show that the blue shift observed in (111) orientation of PS (n- and p- type) is higher than (100). The particle sizes, from both spectra are in good agreement and decreases with increase in etching time. The porosity also shows increase in its value with increase in etching time. The thermal conductivities calculated by photoacoustics are in agreement with the previously reported results [6,10,12] and show that thermal conductivities of p-PS are lower than the n-PS. And the lower thermal conductivity of p-PS in (111) orientation over other samples implies that these samples are the best suitable for thermal insulation in semiconducting devices. The calculated particle size of all the above samples show that they are in nanometer (nm) order implying that the silicon particle size of the porous layers are nanostructurd in nature and this decreases with increasing porosity. Our experimental results on thermal conductivity for all the porous silicon samples are compared with the theoretical model of Looyenga [10], which is quit good. In fact, in recent years, this theory is taken as a standard scale to gauge the experimental results of PS. As already mentioned, this standardization becomes inevitable due to large variations reported in literature for PS.

References

[1] L. T. Canham, Appl. Phys. Lett. **57**, 1046 (1990).
[2] D. J. Lockwood, Solid State Commun. **92**, 101 (1994).
[3] X. Z Tu, J Electrochem. Soc: Solid-State Sci. Technol. **135**, 2105 (1987).
[4] L. T. Canham, Adv. Mater. **7**, 1033 (1995).
[5] I. V. Blonskij, M. S. Brodyn, V. A. Tkhoryk, A. G. Filin, and Ju. P. Piryatinskij, Semicond. Sci. Technology **12**, 11 (1997).
[6] A. Ferreira da Silva, T. Souza da Silva, O. Nakamura, M. M. F. d'Aguiar Neto, I. Pepe, L. S. Roman, and E. Veje, Mat. Res. **4**, 23 (2001).
[7] R. Prabakaran, R. Kesavamoorthy, and Alok Singh, Bull. Matter. Sci. **28**, 219 (2005).
[8] Qing Shen and Taro Toyoda, Rev. Sci. Instr. **74**, 601 (2003).
[9] M. Jayachandran, M. Paramasivam, K. R. Murali, D. C. Trivedi, and M. Raghavan, Mat. Phys. Mech. **4**, 143 (2001).
[10] S. Lettieri, U. Bernini, E. Massera, and P. Maddalena, phys. stat. sol. (c) **2**, 3414 (2005).
[11] J. Ebothe, I. V. Kityk, P. Rocai Cabarrocas, C. Godet, and B. Equer, J. Phys. D: Appl. Phys. **36**, 713 (2003).
[12] L. A. Karachevtseva, O. A. Lytvynenko, E. A. Malovichko, V. D. Sobolev, and O. J. Stronska, Semicond. Phys., Quant. Electron. Optoelectro. **4**, 40 (2001).
[13] Zhao Yue, Li Dong-sheng, Xing Shou-ziang, Yang De-ren, and Jiang Min-hua, J Zhejiang Univ. SCI. **6B**, 1135 (2005).
[14] G. Algun and M. C. Arikan, Tr. J. Phys. **23**, 789 (1999).
[15] M. D. McCluskey, J. Appl. Phys. **87**, 3593 (2000).
[16] A. Rosencwaig, Photoacoustics and Photoacoustic Spectroscopy (Wiley, New York, 1980).
[17] A. Mandells (ed.), Progress in Photothermal and Photoacoustic Science and Technology, Vol. 1 (Elsevier, New York, 1992).
[18] D. Bicanic (ed.), Photoacoustic and Photothermal Phenomenon III (Springer, Berlin, 1992)
[19] A. Rosencwaig, Phys. Today **28**, 23 (1975).
[20] www.ioffe.rssi.ru/SVA/NSM/Semicond/Si/thermal.html.
[21] Fu Ying and Xu Wenlan, Solid State Commun. **62**, 63 (1987).
[22] Jie Zou and Alexander Balandin, J. Appl. Phys. **89**, 2932 (2001).
[23] G. Gesele, J. Linsmeier, V. Drach, J. Fricke, and R. Arens-Fisher, J. Phys. D: Appl. Phys. **30**, 2911(1997).
[24] Y. Wang, A. Suna, W. Mahler, and R. Kasowski, J. Chem. Phys. **87**, 7315 (1987).

